CO_2 dynamics in the Amargosa Desert: Fluxes and isotopic speciation in a deep unsaturated zone

Michelle A. Walvoord and Robert G. Striegl
U.S. Geological Survey, Lakewood, Colorado, USA

David E. Prudic
U.S. Geological Survey, Carson City, Nevada, USA

David A. Stonestrom
U.S. Geological Survey, Menlo Park, California, USA

Received 25 August 2004; revised 18 November 2004; accepted 30 November 2004; published 4 February 2005.

[1] Natural unsaturated-zone gas profiles at the U.S. Geological Survey's Amargosa Desert Research Site, near Beatty, Nevada, reveal the presence of two physically and isotopically distinct CO_2 sources, one shallow and one deep. The shallow source derives from seasonally variable autotrophic and heterotrophic respiration in the root zone. Scanning electron micrograph results indicate that at least part of the deep CO_2 source is associated with calcite precipitation at the 110-m-deep water table. We use a geochemical gas-diffusion model to explore processes of CO_2 production and behavior in the unsaturated zone. The individual isotopic species $^{12}CO_2$, $^{13}CO_2$, and $^{14}CO_2$ are treated as separate chemical components that diffuse and react independently. Steady state model solutions, constrained by the measured P_{CO_2}, $\delta^{13}C$ (in CO_2), and $\delta^{14}C$ (in CO_2) profiles, indicate that the shallow CO_2 source from root and microbial respiration composes ~97% of the annual average total CO_2 production at this arid site. Despite the small contribution from deep CO_2 production amounting to ~0.1 mol m^{-2} yr^{-1}, upward diffusion from depth strongly influences the distribution of CO_2 and carbon isotopes in the deep unsaturated zone. In addition to diffusion from deep CO_2 production, ^{14}C exchange with a sorbed CO_2 phase is indicated by the modeled $\delta^{14}C$ profiles, confirming previous work. The new model of carbon-isotopic profiles provides a quantitative approach for evaluating fluxes of carbon under natural conditions in deep unsaturated zones.

Citation: Walvoord, M. A., R. G. Striegl, D. E. Prudic, and D. A. Stonestrom (2005), CO_2 dynamics in the Amargosa Desert: Fluxes and isotopic speciation in a deep unsaturated zone, *Water Resour. Res.*, *41*, W02006, doi:10.1029/2004WR003599.

1. Introduction

[2] Respiration of plant roots and soil autotrophs varies in response to annual temperature, moisture, and nutrient cycles, causing carbon dioxide (CO_2) concentrations in soil and the upper unsaturated zone to fluctuate seasonally [*Reardon et al.*, 1979; *Thorstenson et al.*, 1983, 1998; *Laursen*, 1991]. These near-surface sources are commonly regarded as the primary contributors of CO_2 to the soil atmosphere and of CO_2 flux across the soil-air interface. CO_2 generated in the soil zone diffuses upward to the atmosphere and, in most cases, diffuses downward to the water table, resulting in essentially uniform P_{CO_2} below the attenuation depth of seasonal fluctuations (~5 to 8 m) [*Reardon et al.*, 1979]. However, many field studies indicate an additional deep CO_2 source originating at or immediately above the water table [*Wood and Petraitis*, 1984; *Striegl and Healy*, 1990; *Keller*, 1991; *Hendry et al.*, 1993; *Lawrence et al.*, 1993; *Wood et al.*, 1993; *Trumbore et al.*, 1995]. Such is the case in the Amargosa Desert, Nevada, where an observed trend of increasing P_{CO_2} with depth through the 110-m-thick unsaturated zone suggests a deep source of CO_2 well below the soil zone [*Stonestrom et al.*, 1999].

[3] The U.S. Geological Survey's Amargosa Desert Research Site (ADRS; Figures 1a and 1b; http://nevada.usgs.gov/adrs/) is an observatory for long-term field studies of unsaturated-zone hydrology under natural and perturbed conditions. This paper uses data from the ADRS and nearby locations to construct unperturbed unsaturated-zone profiles of (total) CO_2, $^{13}CO_2$, and $^{14}CO_2$ from the land surface to the water table. These profiles are likely representative of large interfluvial areas with xeric vegetation in the Amargosa Desert. The gas partial pressure distributions are then simulated using previously determined physical properties of the unsaturated zone [*Fischer*, 1992; *Andraski*, 1997; *Prudic et al.*, 1997] in a coupled geochemical-gas diffusion model that considers the transport properties and geochemical behavior of each isotopic species [*Parkhurst et al.*, 2000]. The influences of the shallow and deep sources on CO_2, $^{13}CO_2$, and $^{14}CO_2$ distributions are then quantified.

[4] The distribution of ^{14}C in the unsaturated zone can have important implications in the calculation of ground-

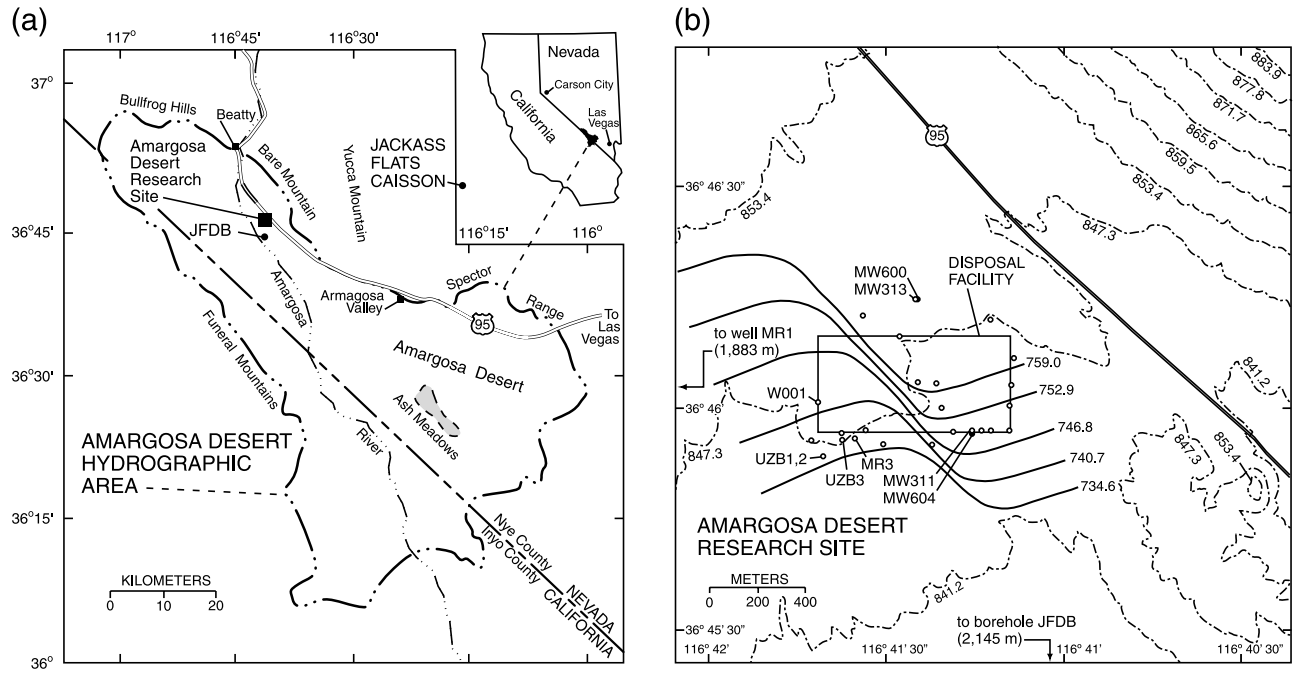

Figure 1. Location of (a) Amargosa Desert hydrographic boundary from *Harrill et al.* [1988] and sample sites, and (b) Amargosa Desert Research Site, showing locations of sampled boreholes and wells and the approximate elevation (in meters above mean sea level) of the water table. Solid lines are elevations of water table contours inferred from water level measurements made by the U.S. Geological Survey (unpublished data) and by U.S. Ecology, Inc. (R. Marchand, personal communication, 2003, 2004). Open circles are control points, wells screened across the water table. Solid circles are wells screened below the water table. Wells from which water samples have been analyzed for C isotopes are labeled. Dash-dotted lines are land surface elevations (in meters above mean sea level).

water ^{14}C dating in certain settings [*Bacon and Keller*, 1998]. Many conventional ^{14}C groundwater age-dating models assume reaction of modern CO_2 from the unsaturated zone with very old (negligible ^{14}C) carbonate in a closed system. Although this approach may be appropriate for regions having unsaturated zones in which CO_2 production is confined to the root zone, it may not be appropriate in systems of active recharge that possess a source of CO_2 depleted in ^{14}C near the water table. Using data from a site in Saskatchewan, *Bacon and Keller* [1998] described how georespiration from a source of Cretaceous-age organic carbon just above the water table results in incorrect groundwater age predictions by applying conventional closed-system ^{14}C dating models. Their work highlighted the importance of assuming open-system equilibrium with the isotopic composition of gas just above the water table. In the absence of deep unsaturated-zone data, prediction of ^{14}C relative to ^{12}C in bulk CO_2 near the water table may be quite difficult. *Thorstenson et al.* [1983] attempted to model the downward transport of atmospheric ^{14}C in an unsaturated zone in North Dakota and found that calcite equilibria, coupled with isotope exchange in a two-phase system, did not adequately explain ^{14}C retardation. *Striegl and Armstrong* [1990] attributed this to a previously unquantified sorbed CO_2 phase. They conducted laboratory experiments on a variety of soil types and found that the retained CO_2 reservoir exceeded the dissolved inorganic carbon (DIC) reservoir by 8–17 times. *Striegl and Healy* [1990] applied sediment specific isotherms from that work to show that similar sorption is occurring in the field. On the basis of a mesoscale experiment, *Plummer et al.* [2004] calculated, from the analysis of breakthrough curves, and directly measured the mass of sorbed ^{14}C that exceeded the mass of ^{14}C in the aqueous reservoir by 2–14 times. Here we test the hypothesis that both a source of CO_2 depleted in ^{14}C near the water table and a generalized ^{14}C sorption isotherm described by *Striegl and Armstrong* [1990] are necessary and sufficient to explain natural ^{14}C distribution in the unsaturated zone at the ADRS.

2. Site and Borehole Description

[5] The ADRS is located in an alluvial basin in the northern Mojave Desert, ~17 km south of Beatty, Nevada (Figure 1a) [*Andraski and Stonestrom*, 1999]. Basin-fill sediments consist predominantly of unconsolidated debris flow, fluvial, and alluvial-fan deposits [*Nichols*, 1987; *Stonestrom et al.*, 2004]. The unsaturated zone is predominantly sand and gravel, ranges from 85 to 115 m thick at the ADRS [*Fischer*, 1992] and is 110 m thick at borehole UZB-2. Precipitation records from 1981 to 2000 show an annual average of 108 mm at the ADRS, of which ~70% arrives in frontal systems during October through April [*Johnson et al.*, 2002]. Annual potential evaporation is 1900 mm [*Nichols*, 1987]. Average monthly temperatures range from 30°C in August to 7°C in December [*Johnson et al.*, 2002]. Major plant species at the ADRS include

creosote (*Larrea tridentata* (*DC*) *Colville*) (70%) and saltbush (*Atriplex confertifolia* (*Torr. & Frem.*) *S.Wats*) (<20%).

[6] The ADRS serves as a field-scale laboratory to investigate complex flow and transport processes in deep arid unsaturated zones under natural and perturbed conditions due to its proximity to a waste-burial facility. The waste facility has been used for the burial of low-level radioactive waste (1962–1992) and hazardous chemical waste (since 1970). Gas-concentration and isotope data compiled for this study are limited to those believed to represent natural (unperturbed) conditions, on the basis of supplemental data from locations outside of the 16-ha ADRS boundary. These sites include the JFDB site, ~3 km to the south, and the Jackass Flats (JF) site, located 35 km to the east (Figure 1a).

3. Methods

3.1. Data Collection and Analyses

[7] The UZB-series boreholes at the ADRS (Figure 1b) were drilled using the air-hammer drilling method [*Hammermeister et al.*, 1985]. Both UZB-3 (December 1999) and UZB-2 (September 1993) were drilled to a depth of 114.6 m. Core samples were collected from both holes and also from UZB-1, the latter drilled in November 1992 to a depth of 48 m and located 6 m southwest of UZB-2. Sections of the cores were analyzed for particle size, bulk density, specific surface area, porosity, water content, water potential, and chloride. Water content measurements were determined by oven-drying core samples [*Prudic et al.*, 1997]. Neutron logging of nearby boreholes has produced a multiyear record of water content profiles [*Fischer*, 1992; *Andraski*, 1997]. Water content changes monitored between 1987 and 1992 were limited to the upper 0.5–1 m [*Andraski*, 1997]. Sections of the core from UZB-3 collected just above and just below the water table were analyzed using scanning electron microscopy (SEM) with electron dispersive spectroscopy to determine the presence and composition of authigenic and detrital minerals. Surface areas of the <1-mm fraction of UZB-1 and UZB-2 samples were determined by multipoint nitrogen adsorption (D. Rutherford, U.S. Geological Survey, unpublished data, 2000).

[8] Gas samples were collected from ports located within instrumented boreholes, UZB-2, JFDB, and JF following the procedures described by *Prudic et al.* [1999] and *Thorstenson et al.* [1998]. Each port consists of a 30-cm-long stainless steel screen connected to 6-mm-diameter nylon tubing that extends to land surface [*Prudic et al.*, 1997]. A total volume of about 100 L of gas was pumped to purge each port prior to sampling [*Prudic and Striegl*, 1995]. Gas samples were analyzed during or within minutes of collection for P_{CO_2} using a portable infrared CO_2 analyzer. Gas compositions of samples were also analyzed by gas chromatography in 1997 [*Stonestrom et al.*, 1999] and 2003 [*Baker et al.*, 2003] with comparable results. To determine isotopic composition, CO_2 was trapped by bubbling soil gas through concentrated KOH or NaOH solutions, precipitated as barium carbonate, then analyzed for ^{13}C and ^{14}C by isotope ratio mass spectrometry and scintillation counting, respectively [*Haas et al.*, 1983; *Stonestrom et al.*, 2001]. The stable carbon isotopic ratio $^{13}C/^{12}C$ in samples, R_{sample}, is reported relative to the $^{13}C/^{12}C$ ratio in Pee Dee belemnite ($R_{STD} = (^{13}C/^{12}C)_{STD} = 0.011237$) [*Craig*, 1957].

$$\delta^{13}C(in\ ‰) = \left(\frac{R_{sample}}{R_{STD}} - 1\right) \times 1000 = \left(\frac{\left(^{13}C/^{12}C\right)_{sample}}{\left(^{13}C/^{12}C\right)_{STD}} - 1\right) \times 1000. \quad (1)$$

The radiocarbon isotopic ratio $^{14}C/^{12}C$ in samples, R_{sample}, is reported relative to the National Institute of Standards and Technology oxalic acid standard decay-corrected to 1950 ($R_{STD} = {}^{14}C/^{12}C_{STD} = 1.176 \times 10^{-12}$) [*Stuiver and Polach*, 1977] and expressed as

$$\delta^{14}C(in\ ‰) = \left(\frac{R_{sample}}{R_{STD}} - 1\right) \times 1000 = \left(\frac{\left(^{14}C/^{12}C\right)_{sample}}{\left(^{14}C/^{12}C\right)_{STD}} - 1\right) \times 1000. \quad (2)$$

[9] Groundwater samples from six monitoring wells at the ADRS, MW313, MW600, MW311, MW604, MR-3, and W001 (Figure 1b), were collected and chemically analyzed between 1989 and 1992. Four of the wells sampled have screens that intersect the water table, and two wells are screened at least 30 m below the water table. Paired wells (MW313 and MW600; MW311 and MW604) were installed at two locations to evaluate shallow and deep groundwater conditions. Wells MW313 and MW600 are upgradient from the waste burial area and samples are not influenced by buried waste. At least three well-bore volumes were removed from each well prior to sample collection. Temperature, pH, specific conductance, dissolved oxygen, and alkalinity were measured at the time of collection. Samples for major ion and trace element analysis were filtered using a 0.45-μm membrane cartridge filter. Samples were stored in polyethylene bottles, and samples for cations and trace elements were acidified to a pH of <2 with nitric acid [*Wood*, 1976]. Samples for DOC were filtered through a 0.45-μm silver membrane filter inside a stainless steel holder, stored in amber glass bottles, and kept chilled at 4°C until analyzed. Samples for ^{14}C analyses were collected in a 2-L linear polyethylene bottle that was attached to the bottom of a 200-L precipitation tank. The tank was flushed with nitrogen gas prior to being filled with water. Dissolved inorganic carbon was converted to CO_3^{-2} at pH greater than 10 by using CO_2-free NaOH and then precipitated as $SrCO_3$ by adding a solution of CO_2-free $SrCl_2$. Samples for ^{13}C analyses were collected by inserting the end of the sample tubing to the bottom of a 1-L glass bottle and flushing the bottle with several volumes of sample water before final collection. A CO_2-free ammoniacal $SrCl_2$ solution was then added to precipitate $SrCO_3$. Suspended particles were removed from both ^{14}C and ^{13}C samples by using an in-line filter closed to the atmosphere. All samples were analyzed at the U.S. Geological Survey's National Water Quality Laboratory.

3.2. Model Description

[10] The numerical model used in this study is a research version of the geochemical code PHREEQC [*Parkhurst*

Table 1. Parameters for All Simulations, Unless Otherwise Noted

Parameter	Value	Comments
Depth to water table, m	110	measured depth at UZB-2
Temperature, °C	25	measured water table temperature
$^{12}CO_2$ diffusion coefficient in air, $m^2\ s^{-1}$	1.650×10^{-5}	value at 25°C and 0.1 MPa
$^{13}CO_2$ diffusion coefficient in air, $m^2\ s^{-1}$	1.643×10^{-5}	calculated from fractionation factor of *Deines et al.* [1974]
$^{14}CO_2$ diffusion coefficient in air, $m^2\ s^{-1}$	1.634×10^{-5}	calculated from fractionation factor of *Deines et al.* [1974]
Freundlich isotherm parameter K_f, mol C m^{-2} Pa^{-1}	3.8×10^{-10}	*Striegl and Armstrong* [1990]
Freundlich isotherm parameter n	0.85	*Striegl and Armstrong* [1990]
Sediment surface area per total mass, $m^2\ g^{-1}$	10	derived from D. Rutherford (unpublished data, 2000)

and Appelo, 1999] coupled with a finite difference gas-diffusion algorithm in which $^{12}CO_2$, $^{13}CO_2$, and $^{14}CO_2$ are treated as individual chemical entities that diffuse and react independently [*Parkhurst et al.*, 2000]. They are defined as separate components in the ion-association geochemical model PHREEQC, with appropriate thermodynamic equilibrium constants for gaseous and aqueous species of each isotopic variant. Equilibrium constants were derived by *Thorstenson and Parkhurst* [2004] by extending the work of *Urey* [1947]. Experimental fractionation factors used in derivations were taken from *Deines et al.* [1974].

[11] Retention of CO_2 in the porous medium was considered by specifying gas sorption according to the Freundlich isotherm:

$$q = K_F(P_{CO_2})^n, \tag{3}$$

where, q is the amount of sorbed [mol CO_2 m^{-2} sediment], K_F is the Freundlich partitioning coefficient [mol CO_2 m^{-2} Pa^{-1}], P_{CO_2} is partial pressure of CO_2 [Pa], and n is the Freundlich exponent. Sorption of C isotopes was handled by assuming isotopic equilibrium between the gaseous and aqueous plus adsorbed phases of C species [cf. *Striegl and Healy*, 1990].

[12] The model includes a stagnant water phase that is assumed to be always in chemical and isotopic equilibrium with the gas phase. The numerical algorithm uses sequential iteration between (1) the gas-transport calculation and (2) the geochemical-reaction and gas-water-equilibrium calculation. Sequential iterations for a time step are complete when the reaction terms in the transport equation produce gas-water equilibrium for each gas component within specified tolerances.

3.3. Model Application

[13] The model described above was applied to the ADRS site to simulate CO_2 dynamics in a 110-m-thick unsaturated zone. The main parameters used in the model are given in Table 1. Isothermal conditions of 25°C are assumed for modeling purposes. The free air diffusion coefficients for each isotopic component of CO_2 are provided in Table 1. Specified values of Freundlich isotherm constants derived from *Striegl and Armstrong* [1990] are listed in Table 1. Prescribed porosities and volumetric water contents vary with depth through the 110-m model column according to measurements of the unsaturated zone at UZB-2 (Figure 2). Water contents in UZB-2 are relatively well constrained to a depth of 94 m and are assumed to be invariant, as supported by neutron data that indicate annual water-content changes are confined to the upper 0.5–1 m [*Andraski*, 1997]. Porosities, particularly at depth, are relatively poorly constrained because of the difficulty of obtaining bulk density from core samples in gravelly sediments. Main sources of uncertainty among model parameters include porosity and water content at depth, which together determine the air content (a). As shown in Figure 2, the ratio of the effective gas diffusion coefficient (D) to the

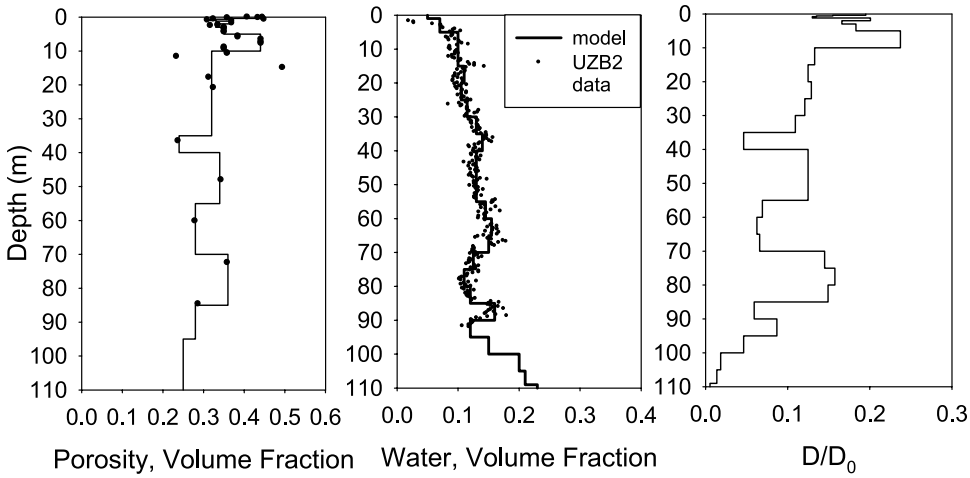

Figure 2. Distributions of porosity, water content, and the gas diffusivity ratio (D/D_0) that were used as model input. Porosity and water content distributions were based on data and lithologic logs from UZB-2. Porosities were calculated from bulk density measurements.

Table 2. Boundary Conditions and Source Terms for Base-Case Steady State Simulation

Boundary Conditions and Source Terms	Value	Comments
Fixed surface CO_2, Pa	38	atmospheric value
Fixed surface $\delta^{13}C$ in CO_2, ‰	−8.5	atmosphere at Yucca Mountain Crest, 1987–1993 average[a]
Fixed surface ^{13}C in CO_2, ‰	185	atmospheric value at Yucca Mountain Crest, 1992[a]
CO_2 soil respiration, mol m^{-2} yr^{-1}	3.0	estimated[b]; uniformly distributed in upper 1 m
$\delta^{13}C$ of soil respiration, ‰	−27	value of soil organic matter and depleted by 4.4‰[c]
$\delta^{14}C$ of soil respiration, ‰	200	fitting parameter; within range of 1984–1992 atmospheric values[a]
CO_2 deep production, mol m^{-2} yr^{-1}	0.10	fitting parameter
$\delta^{13}C$ of deep CO_2, ‰	−17.6	gas in isotopic equilibrium (−13.2‰) with MW313 groundwater (−6.2‰) and depleted by 4.4‰[c]
$\delta^{14}C$ of deep CO_2, ‰	−880	gas in isotopic equilibrium with MW313 groundwater (−880‰)

[a]From *Thorstenson et al.* [1998].
[b]From T. A. McConnaughey (unpublished data, 1993).
[c]A 4.4‰ depletion correction for $\delta^{13}C$ between soil gas CO_2 concentration and CO_2 flux described by *Cerling et al.* [1991].

free air diffusion coefficient (D_0) varies as a function of a according to the *Millington* [1959] equation:

$$\frac{D}{D_0} = a^{4/3}. \quad (4)$$

[14] The model simulates CO_2 production in the root zone (0- to 1-m depth interval) and at 0 to 1 m above the water table. The prescribed deep CO_2 flux and its isotopic composition were varied within reasonable ranges to produce the best fits to the observed P_{CO_2}, $\delta^{13}C$, and $\delta^{14}C$ profiles by trial and error. Model simulations were run to steady state. The set of boundary conditions consisting of the combination of available measurements and fitted parameters, where measurements are not available, that produce the best match to ADRS profile data is referred to as the "base case" (Table 2). The base-case simulation serves as a standard for evaluating the effects of unsaturated-zone parameters, boundary conditions, and source terms on P_{CO_2}, $\delta^{13}C$, and $\delta^{14}C$ profiles. The steady state results from the base-case simulation supplied the initial condition for transient simulations to address seasonal-annual variations in soil respiration. Transient simulations establish how deeply near-surface changes in P_{CO_2} and $\delta^{13}C$ propagate as a function of time.

[15] Several boundary conditions in the base case (Table 2) were taken from measured CO_2 fluxes and $\delta^{13}C$ and $\delta^{14}C$ values in the upper 10 m of the unsaturated zone at Jackass Flats (JF) [*Thorstenson et al.*, 1998]. In addition, the 1984–1993 record of $\delta^{14}C$ in atmospheric CO_2 measured at Yucca Mountain Crest (YMC) [*Thorstenson et al.*, 1998] was used to establish the recent history of atmospheric radiocarbon (Figure 3).

4. Results and Discussion

4.1. Observed P_{CO_2}, $\delta^{13}C$, and $\delta^{14}C$ Deep Unsaturated-Zone CO_2 Profiles

[16] Composite unsaturated-zone gas analyses from the UZB-2, JFDB, and JF boreholes (Figure 4) show a consistent increase of CO_2 partial pressure with depth indicating a deep source of CO_2 [*Prudic and Striegl*, 1994]. The maximum P_{CO_2}, of ~1000 Pa, is observed just above the water table. To a lesser degree, the $\delta^{13}C$ in CO_2 also increases with depth. In contrast, the composite $\delta^{14}C$ in CO_2 decreases from +200‰ near the land surface to −880‰ just above the water table [*Stonestrom et al.*, 2001]. The $\delta^{14}C$ values from land surface to 30 m were taken from JFDB, located ~3 km from the ADRS. These values were used to generate the "undisturbed" $\delta^{14}C$ 1992 profile because the upper part of the UZB-2 profile showed signs of ^{14}C contamination [*Striegl et al.*, 1996]. The 1992 $\delta^{14}C$ values from the 10-m-deep research shaft at Jackass Flats (reported by *Thorstenson et al.* [1998]) were included to generate the composite profile.

4.2. Soil Respiration

[17] Both concentration and isotopic composition of CO_2 in the soil zone of the Amargosa Desert vary seasonally and interannually, as illustrated by P_{CO_2} and $\delta^{13}C$ of CO_2 profiles collected adjacent to UZB-2 at multiple dates during 1993 [*McConnaughey et al.*, 1994; T. A. McConnaughey, unpublished data, 1993] and at JF during 1987, 1988, 1989, and 1992 [*Thorstenson et al.*, 1998]

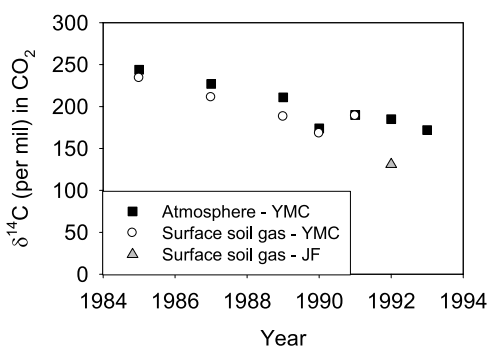

Figure 3. Record of $\delta^{14}C$ measured in CO_2 in atmospheric and surface soil gas at Yucca Mountain Crest (YMC) and Jackass Flats (JF), from *Thorstenson et al.* [1998].

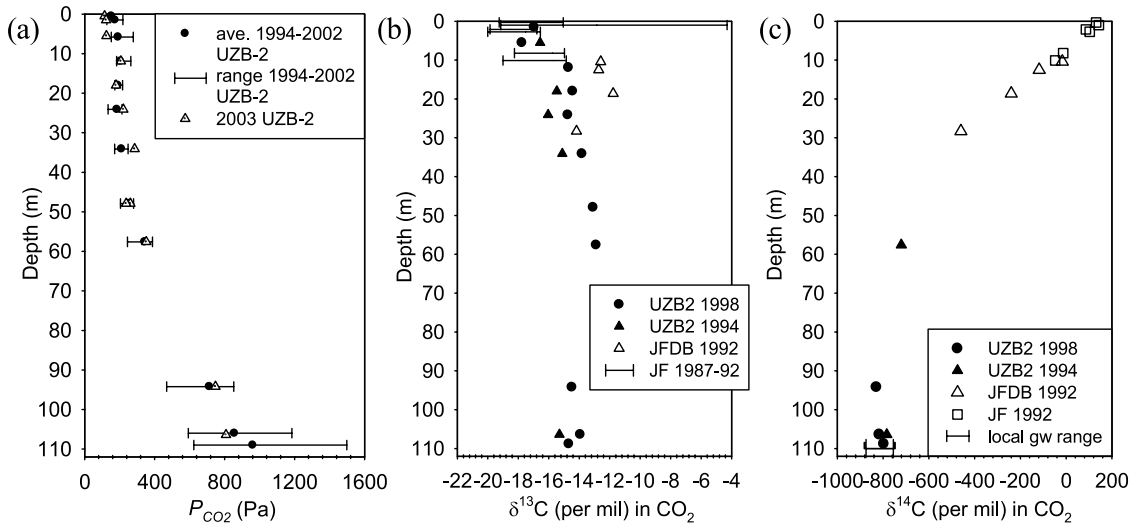

Figure 4. Data from UZB-2 at the Amargosa Desert Research Site (ADRS), JFDB located ~3 km from the ADRS, and Jackass Flats (JF) located 35 km east of the ADRS. Profiles considered in this study include (a) soil P_{CO_2} (b) δ^{13}C, and (c) δ^{14}C. JF data are given by *Thorstenson et al.* [1998].

(Figure 5). These data were used to determine the range of soil respiration rates for the UZB-2 model simulations. Soil respiration values from flux-chamber measurements collected continuously during the1998 El Niño year at the JFDB site [*Riggs et al.*, 1999] were used to constrain the production rate for the wet condition. Total precipitation during 1998 was 180% above the 20-year (1981–2000) annual average [*Johnson et al.*, 2002]. Daily soil respiration peaked at 20 mol CO_2 m^{-2} yr^{-1} in the spring of 1998 around Julian Day 120 and remained at or below ~7 mol CO_2 m^{-2} yr^{-1} for the rest of the year [*Riggs et al.*, 1999]. Accordingly, shallow production of 7 mol CO_2 m^{-2} yr^{-1} was used as the upper-end value for the steady state simulations. The 1998 JFDB soil respiration exceeded both the 1993 estimate for the ADRS (~3.0 mol CO_2 m^{-2} yr^{-1}) and the 7-year average estimated for Jackass Flats (3.5 mol CO_2 m^{-2} yr^{-1} [*Thorstenson et al.*, 1998]) by a factor of 2.

[18] Microbial respiration between the bottom of the soil zone and above the capillary fringe is much less than soil respiration rates [*Konopka and Turco*, 1991; *Wood et al.*, 1993]. Low microbial counts, $<4 \times 10^3$ colony-forming units per gram of sediment (CFU g^{-1}), between depths of 5 and 80 m in UZB-3 support the assumption of low biological activity in this interval [*Stonestrom et al.*, 2001]. Microbial counts from UZB-3 increase to 10^5 CFU g^{-1} above the water table and 10^6 CFU g^{-1} at 2 m below the water table. For reference, *Kieft et al.* [1995] reported basal respiration rates (an upper-end estimate of in situ rates) of

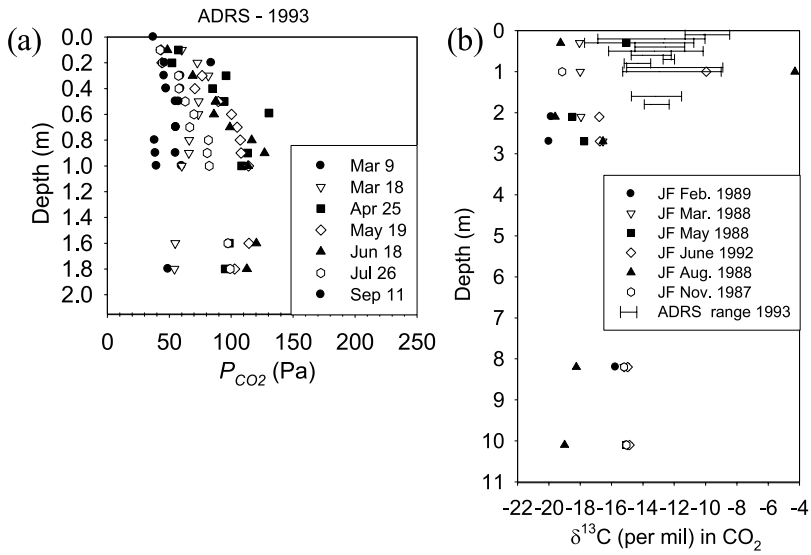

Figure 5. Data applied to the model analyses, including (a) shallow soil P_{CO_2} at the ADRS adjacent to UZB-2, and (b) δ^{13}C from the ADRS and Jackass Flats (JF). ADRS data are from T. A. McConnaughey (unpublished data, 1993), and JF data are from *Thorstenson et al.* [1998].

Table 3. Chemical (Major Constituents) and Carbon Isotopic Composition of Groundwater From Wells Near the ADRS Depicted in Figure 1

Sample	MW313	MW600 (Deep)	MW311	MW604 (Deep)	MR-3	W001
Date sampled	08/15/89	12/08/92	12/09/92	12/09/92	08/16/89	12/08/92
Land surface elevation, m[a]	848.5	848.4	844.7	844.3	846.5	848.5
Screened interval elevation, m[a]	762.5–756.5	707.4–704.4	753.7–746.7	718.3–714.3	735.5–723.5	744.5–736.5
Static water elevation, m[a]	760.7	755.1	751.7	744.9	734.3	743.3
Temperature, °C	24.5	24.5	24.5	25.0	28.5	23.0
pH	7.70	7.99	7.76	8.18	7.51	7.70
Dissolved oxygen, mg L^{-1}	5.4	4.2	6.0	4.8	5.4	6.5
Organic carbon, mg L^{-1}	0.5	0.4	3.1	1.3	0.8	38[b]
Nitrate + nitrite as N, mg L^{-1}	0.19	0.23	0.22	0.21	0.22	0.31
Ortho phosphorus, mg L^{-1}	<0.02[c]	0.008	0.007	0.008	<0.02[c]	0.004
Calcium, mg L^{-1}	50	19	48	26	47	53
Magnesium, mg L^{-1}	16	11	15	14	18	16
Sodium, mg L^{-1}	170	170	160	180	160	150
Potassium, mg L^{-1}	11	9	10	10	11	11
Bicarbonate, mg L^{-1}	320	288	348	300	320	324
Chloride, mg L^{-1}	70	72	83	72	79	74
Sulfate, mg L^{-1}	210	150	190	170	190	200
Silica, mg L^{-1}	73	58	62	69	67	67
Barium, mg L^{-1}	0.032	0.018	0.021	0.024	0.025	0.024
Boron, mg L^{-1}	0.63	0.67	0.61	0.64	0.57	0.61
Iron, mg L^{-1}	0.034	0.180	0.017	0.120	0.006	0.024
Strontium, mg L^{-1}	0.450	0.350	0.350	0.440	0.370	0.380
Fluoride, mg L^{-1}	3.1	3.3	3.7	3.1	3.4	3.1
Lithium, mg L^{-1}	0.280	0.130	0.230	0.180	0.250	0.240
Bromide, mg L^{-1}	0.280	0.290	0.350	0.290	0.300	0.310
$\delta^{13}C$, ‰	−6.2	−8.1	−6.5	−7.8	−6.7	−6.7
$\delta^{14}C$, ‰	−880	−830	−830	−860	−740	−750

[a]Elevations in meters above mean sea level.
[b]High DOC value ascribed to residual organic foam used to drill well in 1990.
[c]Values below detection limit.

0.3–10.2 mol CO_2 m^{-2} yr^{-1}on fluvial sand samples collected from depths of 193–197 m with $<4 \times 10^4$ CFU g^{-1}. Respiration is highly dependent on carbon availability as well as other factors, and thus microbial counts do not translate directly into respiration rates [*Wood et al.*, 1993]. Nevertheless, the elevated microbial counts near the water table raise the possibility that microbial activity contributes to deep CO_2 production at the ADRS.

4.3. Groundwater Geochemistry and Hydraulics

[19] Relevant geochemical and isotopic analyses of groundwater at the ADRS are presented in Table 3. Samples were low in DOC from all wells except W001, which was drilled using organic foam. Concentrations of dissolved oxygen, calcium, bicarbonate, and sulfate were higher, and pH and iron were lower in the water table wells than in the wells screened deep below the water table. Values of $\delta^{13}C$ in DIC are lighter in deeper groundwater (−7.8 and −8.1‰) than in groundwater at the water table (−6.5 and −6.2‰).

[20] The paired wells are northeast of a northwest trending offset in water table contours (Figure 1b). Static water levels at the paired wells indicate a downward hydraulic gradient (Table 3); however, NETPATH [*Plummer et al.*, 1994] simulations are inconsistent with vertical flow. These indicate that water at the water table is from a different source (i.e., is on a different flow line) than water at depth. Shallow groundwater may derive from the Amargosa channel, to the northwest, whereas deeper groundwater may derive from the mountain block, to the northeast (Figure 1a).

[21] Multiple lines of evidence indicate that recharge has been negligible through the thick unsaturated zone at the ADRS for many thousands of years [*Prudic*, 1994; *Walvoord et al.*, 2004] and that local groundwater is at least several thousand years old [*Prudic and Striegl*, 1995; *Stonestrom et al.*, 1999]. Although deep percolation is presently occurring beneath the ephemeral channel of the Amargosa River northwest of the ADRS [*Stonestrom et al.*, 2004], the estimated travel time for infiltrating water to reach the 100-m-deep water table and move laterally to the ADRS is several hundred years. This estimate uses deep percolation rates from *Stonestrom et al.* [2004], the measured groundwater gradient of 0.018 m m^{-1} near W001 (Figure 1b), the measured hydraulic conductivity of 1 m d^{-1} [*Kaufmann and Nacht*, 1989], and an assumed porosity of 0.2 between the river channel and the ADRS.

[22] The lack of current recharge at the site and the relatively long travel time for groundwater imply a low supply of nutrients for microbes in the deep unsaturated zone and in groundwater. Dissolved organic carbon (DOC) levels in groundwater are low (Table 3). Organic carbon at depth likely persists in refractory compounds that are not bioavailable.

[23] Saturation indices calculated with the speciation model WATEQF [*Plummer et al.*, 1976] indicate that the groundwater is supersaturated with respect to calcite and dolomite (Table 4). The log P_{CO_2} of −2.0 at well MR-3 (Table 4) is consistent with CO_2 outgassing from groundwater to the unsaturated zone on the basis of the deep CO_2 profile at borehole UZB-2.

Table 4. Saturation Indices and Calculated Log Partial Pressure of Carbon Dioxide for Groundwater Samples Collected From Wells Near the ADRS as Depicted in Figure 1[a]

	Saturation Index (Log IAP/KT)					
	MW313	MW600 (Deep)	MW311	MW604 (Deep)	MR-3	W001
Calcite	0.40	0.17	0.32	0.49	0.16	0.33
Dolomite	0.63	0.43	0.47	1.06	0.28	0.46
Siderite	−0.94	0.24	−0.72	0.21	−1.59	−0.88
Strontianite	−1.28	−1.11	−1.28	−0.82	−1.51	−1.35
Witherite	−3.48	−3.36	−3.40	−3.05	−3.65	−3.52
Celestite	−2.01	−2.05	−1.87	−1.93	−1.98	−1.96
Gypsum	−1.59	−2.04	−1.53	−1.87	−1.60	−1.52
Fluorite	−0.15	−0.61	−0.29	−0.56	−0.28	−0.24
Quartz	1.0	0.97	1.07	1.03	0.98	1.06
SiO_2(a)	−0.20	−0.30	−0.27	−0.24	−0.27	−0.23
P_{CO_2}	−2.25	−2.56	−2.23	−2.74	−2.01	−2.23

[a]SI > 0 reflects supersaturation (chemical precipitation expected); Saturation index < 0 reflects subsaturation (dissolution expected).

[24] Scanning electron micrograph (SEM) images and electron dispersive spectroscopy (EDS) results from a core collected 2 m below the water table at UZB-3 provide direct evidence of calcite precipitation at the water table beneath the ADRS (Figure 6). Production of CO_2 accompanies calcite precipitation according to the reaction

$$Ca^{2+}_{(aq)} + 2HCO^{-}_{3(aq)} \Leftrightarrow CO_{2(g)} + H_2O_{(l)} + CaCO_{3(s)}. \quad (5)$$

The SEM images confirm the WATEQF inferences of calcite precipitation and outgassing of CO_2 from groundwater. Authigenic calcite is abundant in the capillary fringe; however, incised planar features in some images suggest dissolution and the possibility that authigenic calcite redissolves to some extent during drainage associated with water table declines induced by the current arid climate. CO_2 derived from calcite precipitation near the water table is a source of deep CO_2 production in the thick unsaturated zone at the ADRS. The possibility of a microbial source is discussed in section 5.

4.4. Steady State Model Simulation Results

[25] Simulation results for the steady state base case (using values given in Table 1 and Table 2 as described in section 3) reproduce the unsaturated zone P_{CO_2}, $\delta^{13}C$, and $\delta^{14}C$ profiles from UZB-2 and nearby cores reasonably well (Figure 7). The deep CO_2 production that reasonably fit all profiles was 0.1 mol m^{-2} yr^{-1} (assuming a uniform source

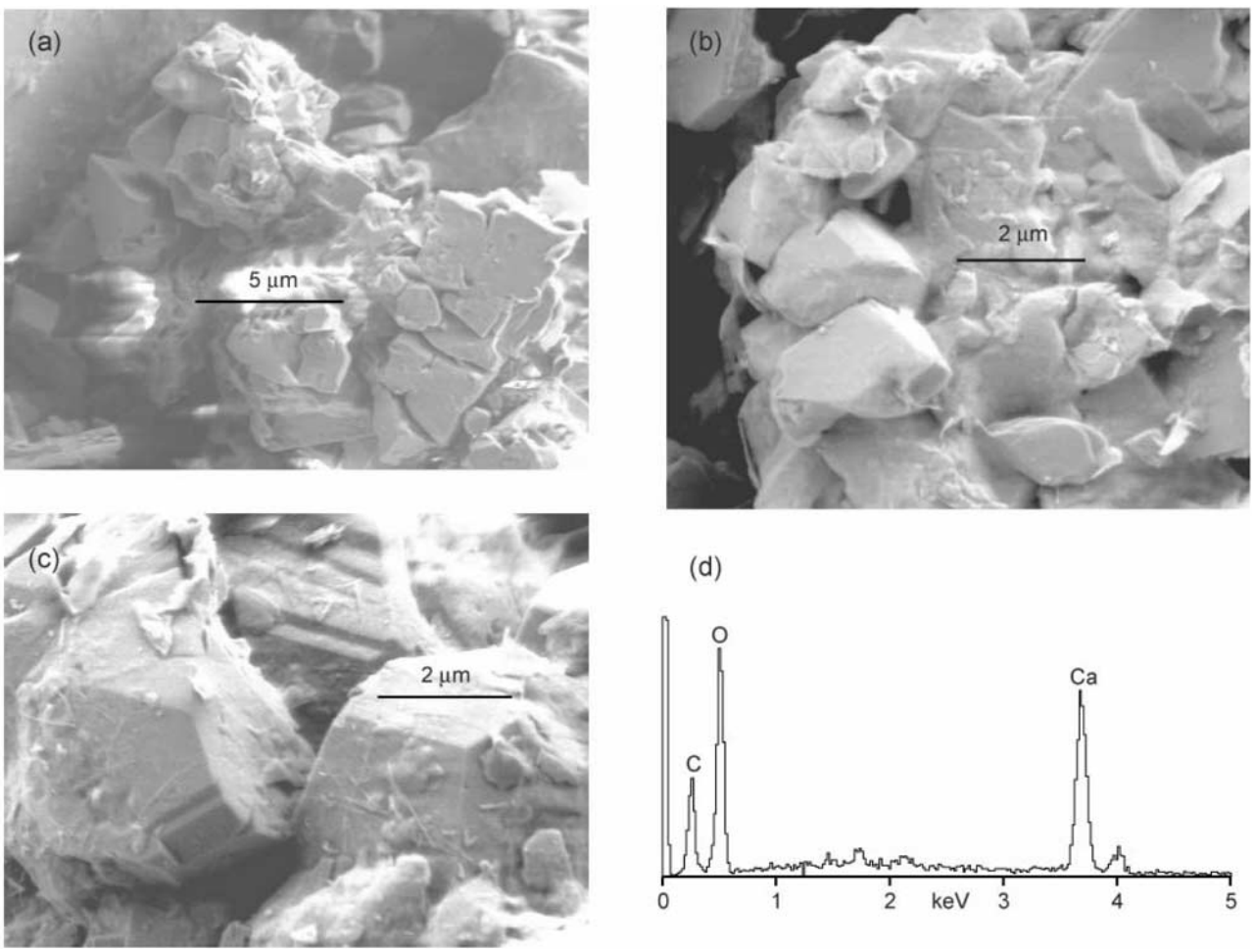

Figure 6. Scanning electron micrographs of authigenic calcite rhombs from UZB-3 core samples (a) ~0.5 m above and (b and c) ~2 m below the water table; (d) electron-dispersive spectrograph of rhombs pictured in Figure 6c.

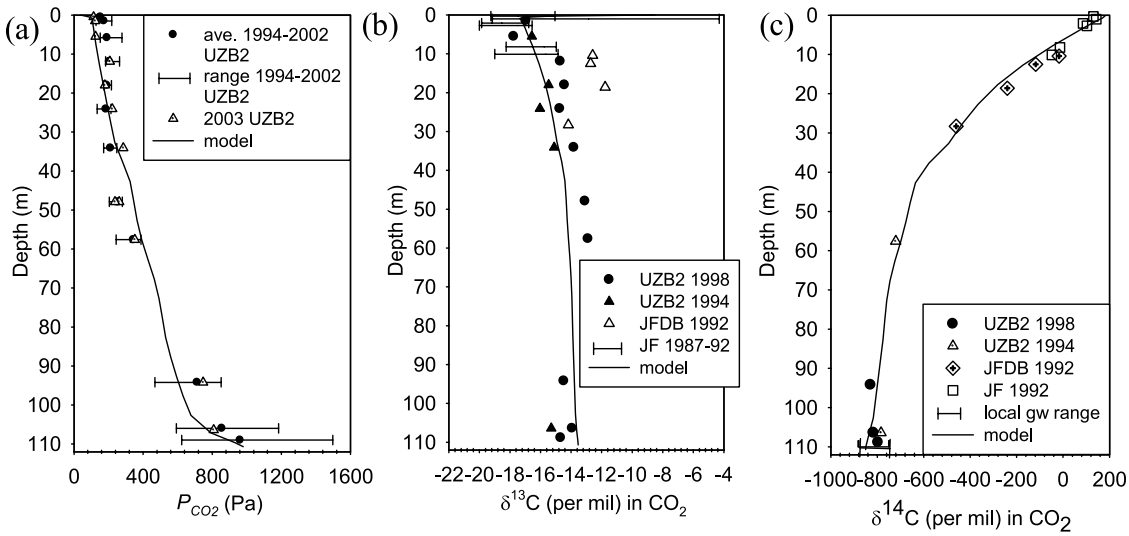

Figure 7. Comparison of modeled steady state (a) P_{CO_2}, (b) $\delta^{13}C$, and (c) $\delta^{14}C$ profiles for the base case to observations. Horizontal bars in Figure 7a represent the range in P_{CO_2} measured in UZB-2 during 1994–2002, and in Figure 7b represent the range in $\delta^{13}C$ measured in the Jackass Flats caisson [*Thorstenson et al.*, 1998] during 1987–1992.

between 0 and 1 m above the water table). Deep production of CO_2 with −17.4‰ $\delta^{13}C$ yields soil gas concentrations above the water table with ∼−13‰ $\delta^{13}C$, consistent with diffusion-related fractionation theory [*Cerling et al.*, 1991]. The diffusion coefficient of $^{12}CO_2$ exceeds that of $^{13}CO_2$ by 4.4‰, thereby enriching the soil gas composition by 4.4‰ relative to the isotopic composition of the source flux. In contrast, enrichment of $^{14}CO_2$ due to diffusion-related fractionation (8.8‰) relative to the 1000‰ difference observed between the upper and lower unsaturated zone was assumed negligible for modeling purposes.

[26] The measured and simulated $\delta^{14}C$ profile in Figure 7c decreases with depth. Note, however, that the partial pressure of $^{14}CO_2$, which is the product of the ^{14}C activity and P_{CO_2}, increases with depth due to the dominant influence of the P_{CO_2} increase (Figure 8a). Although the ^{14}C activity decreases two orders of magnitude with depth, the upward $P_{14_{CO_2}}$ gradient indicates that modern $^{14}CO_2$ is not moving downward in the profile. Rather, older $^{14}CO_2$ is moving upward, resulting in an "older" ^{14}C profile than would exist in the absence of deep CO_2 production in isotopic equilibrium with groundwater. Sorption of $^{14}CO_2$, applied using the generalized sorption isotherm described by *Striegl and Armstrong* [1990], is required to explain the distribution of ^{14}C in the unsaturated zone at the ADRS, especially below 20 m (Figure 8b), thereby demonstrating the transferability of the empirical sorption

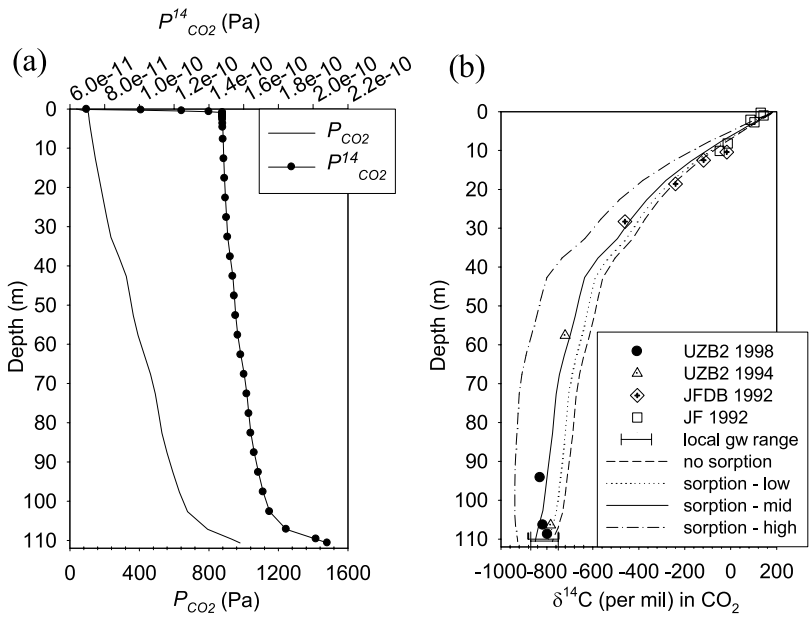

Figure 8. Modeled steady state (a) P_{CO_2} (bottom axis) and $P_{14_{CO_2}}$ (top axis) profiles for the base case, and (b) $\delta^{14}C$ profiles without sorption and for variable degrees of gas sorption based on low (2 m^2 g^{-1}), middle (10 m^2 g^{-2}; used in the base case), and high (20 m^2 g^{-1}) estimates of specific surface area.

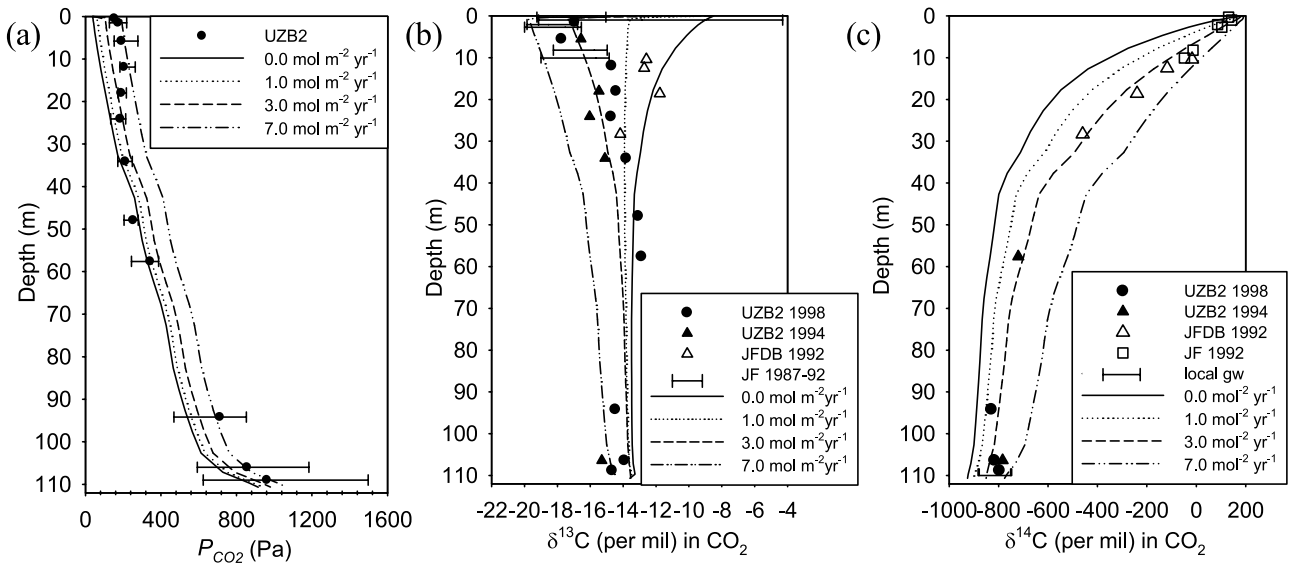

Figure 9. Modeled steady state results displaying the effect of variable shallow CO_2 respiration rates ranging from 0 to 7 mol m^{-2} yr^{-1} on (a) P_{CO_2}, (b) $\delta^{13}C$, and (c) $\delta^{14}C$ profiles.

expression. The $\delta^{14}C$-modeled profiles are relatively sensitive to specific surface area as incorporated in the isotherm [*Striegl and Armstrong*, 1990].

4.4.1. Profile Sensitivity to Soil Respiration Rate

[27] One of the main objectives of the modeling was to estimate approximate rates of CO_2 production in the unsaturated zone. In regard to this objective, sensitivity of fluxes and isotopic profiles to shallow and deep CO_2 source production rates and distribution merits examination. Model sensitivity places constraints on CO_2 source terms, particularly the deep CO_2 production that lacks independent estimates.

[28] As discussed in section 4.2, average shallow CO_2 respiration is constrained by data to be about 3 mol m^{-2} yr^{-1}. Shallow CO_2 respiration varies seasonally and on an annual basis. To evaluate the effects of shallow CO_2 production, the base case was modified to simulate variable CO_2 respiration rates ranging from 0 to 7 mol m^{-2} yr^{-1}. An increased CO_2 respiration rate results in (1) an incremental increase in P_{CO_2} values throughout the entire unsaturated zone (Figure 9a), (2) an isotopic depletion in $\delta^{13}C$ particularly in the upper part of the profile (Figure 9b), and (3) a shift in the $\delta^{14}C$ values toward a "younger" (values closer to 0‰) profile (Figure 9c). The simulation that uses a CO_2 respiration rate of zero represents an extreme end-member. In this case, CO_2 is enriched in $\delta^{13}C$ in the shallow unsaturated zone, approaching atmospheric concentrations. P_{CO_2} also approaches atmospheric concentrations in the shallow unsaturated zone when soil respiration is zero. The $\delta^{14}C$ model simulation results for the zero soil respiration case show the "oldest" (most depleted) $\delta^{14}C$ profile resulting from an upward gradient of $P_{14_{CO_2}}$ that moves older CO_2 (i.e., −880‰ CO_2, in equilibrium with early Holocene groundwater) upward, and is countered by the modern atmospheric reservoir (but not by root-zone production of modern CO_2).

[29] Subtle differences in simulated profiles also result when the distribution of soil respiration is modified. Soil respiration end-members consist of (1) a uniform distribution in the upper 1 m (used in the base case) and (2) a single point distribution at a depth of 1 m. A simulation using a point source of 3 mol m^{-2} yr^{-1} at a depth of 1 m (not shown in the figures) rather than a uniformly distributed source between 0 and 1 m produces a similar effect on the P_{CO_2}, $\delta^{13}C$, and $\delta^{14}C$ profiles as does increasing the uniformly distributed soil respiration rate in the upper 1 m between 3 and 5 mol m^{-2} yr^{-1}.

[30] The isotopic signature of the shallow source also affects the $\delta^{13}C$ and $\delta^{14}C$ in CO_2 profiles. The $\delta^{13}C$ of soil respiration typically ranges from −20 to −27‰ and is related to the composition of organic matter in the soil and of root respired CO_2. Respired CO_2 will be depleted in $\delta^{13}C$ by ∼4.4‰ from the soil gas composition [*Cerling et al.*, 1991]. Steady state simulations with variable soil respiration $\delta^{13}C$ values are shown in Figure 10a. The results indicate the possibility of organic matter that is enriched relative to that assumed for the base case. More likely though, the spread in the $\delta^{13}C$ data in the upper 30 m reflects seasonal and annual fluctuations in soil respiration rates as demonstrated by transient simulations discussed in section 4.5. The $\delta^{14}C$ in the soil zone reflects a mixture of root-respired CO_2 (with $\delta^{14}C$ equal to that of the atmosphere) and bacteria-respired CO_2 (with $\delta^{14}C$ equal to decomposing soil organic matter). The $\delta^{14}C$ of soil organic matter reflects its "age" and formation time [*Wang et al.*, 1996]. Atmospheric $\delta^{14}C$ levels, which peaked at ∼1000‰ in the mid 1960s due to nuclear weapons testing, are still above levels prior to bomb testing (∼80‰ in 2003). Simulations incorporating $\delta^{14}C$ soil respiration values ranging from 0 to 600‰ are shown in Figure 10b. The best fit to the $\delta^{14}C$ unsaturated-zone profile measured in 1992 requires a value of ∼200‰ for the ^{14}C of respired CO_2. This value reflects local atmospheric $\delta^{14}C$ levels in 1989 (Figure 3). If all soil respiration were derived from microbial decomposition of soil organic material, the results would indicate a 3-year average age of labile carbon in the soil. More likely, root respiration contributes substantially to the total soil respiration, which allows for a slightly older average

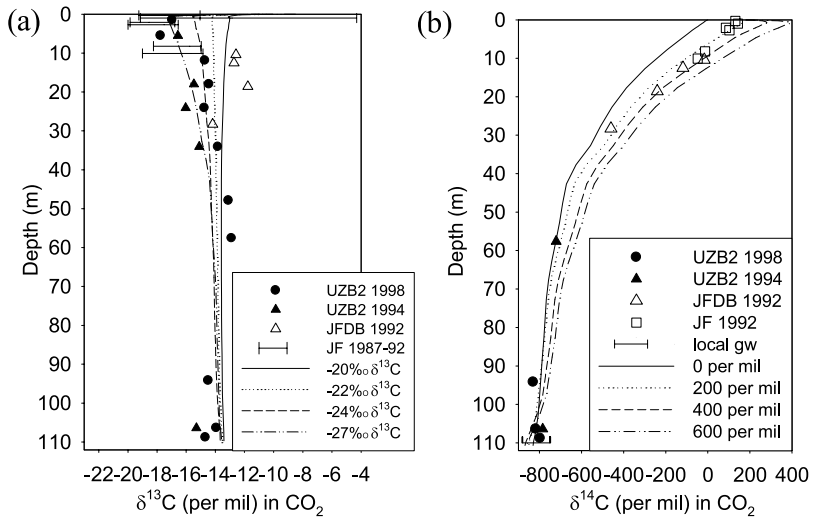

Figure 10. Modeled steady state results displaying the effects of variable (a) $\delta^{13}C$ and (b) $\delta^{14}C$ values of respired CO_2.

labile carbon age (but not exceeding 10 years). Although even older, more recalcitrant carbon sources may dominate soil stores [*Trumbore*, 2000], these results imply that the residence time of labile carbon is not more than ~10 years at the ADRS. This compares to 6–11 years in soils with <5% clay and mean annual temperatures between 20° and 25°C [*Schimel et al.*, 1994].

4.4.2. Deep CO_2 Production Rate

[31] To evaluate the effects of the deep CO_2 source, the base case was modified to simulate variable CO_2 production rates, in the 0- to 1-m interval above the water table, ranging from 0 to 0.14 mol m^{-2} yr^{-1}. Even though the deep source comprises <5% of the total unsaturated-zone CO_2 production within this range, large responses in the P_{CO_2}, $\delta^{13}CO_2$, and $\delta^{14}C$ profiles result by varying the deep production rate (Figure 11). Increasing the deep CO_2 production from 0 to 0.14 mol m^{-2} yr^{-1} results in a shift from a uniform P_{CO_2} profile to curved P_{CO_2} profiles that display marked increases at depth. Larger deep CO_2 production rates cause an isotopic enrichment of $\delta^{13}C$ in CO_2 resulting from the enriched source at depth. The CO_2 produced above the water table is assumed to be in equilibrium with groundwater $\delta^{14}C = -880‰$, so increased deep production results in "older" ^{14}C profiles (Figure 11c). The high degree of sensitivity of the concentration and isotopic distributions of CO_2 to the deep CO_2 production rate imparts confidence in the fitted production term from the model results, given that the deep source is confined to a relatively small (1-m) interval above the water table.

[32] To explore the possibility that the deep CO_2 production is distributed throughout the unsaturated zone at the ADRS, the base case was modified by considering uniform production in the 5- to 110-m interval. CO_2 production throughout the unsaturated zone would indicate microbial activity, calcite precipitation along the vertical temperature gradient, or both. Arguing against these possibilities, the modeled P_{CO_2} profiles for uniform CO_2 production in the range 0.1–5.0 mmol m^{-3} yr^{-1} do not fit the measured profiles (Figure 12a). A larger, relatively discrete source near the water table is required to explain the P_{CO_2}

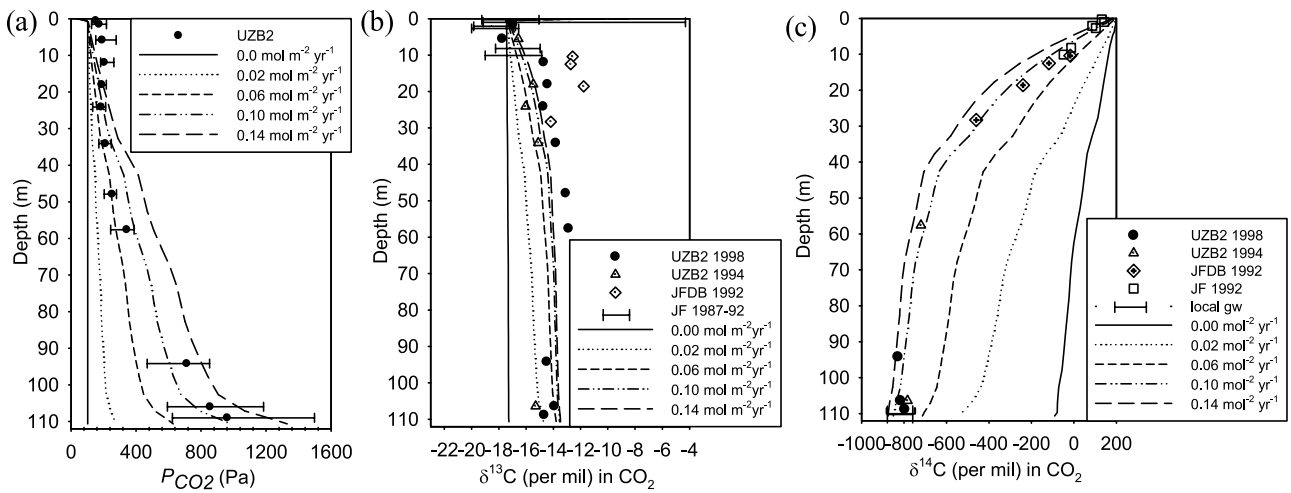

Figure 11. Modeled steady state results displaying the effect of variable deep CO_2 production rates ranging from 0 to 0.14 mol m^{-2} yr^{-1} on (a) P_{CO_2}, (b) $\delta^{13}C$, and (c) $\delta^{14}C$ profiles.

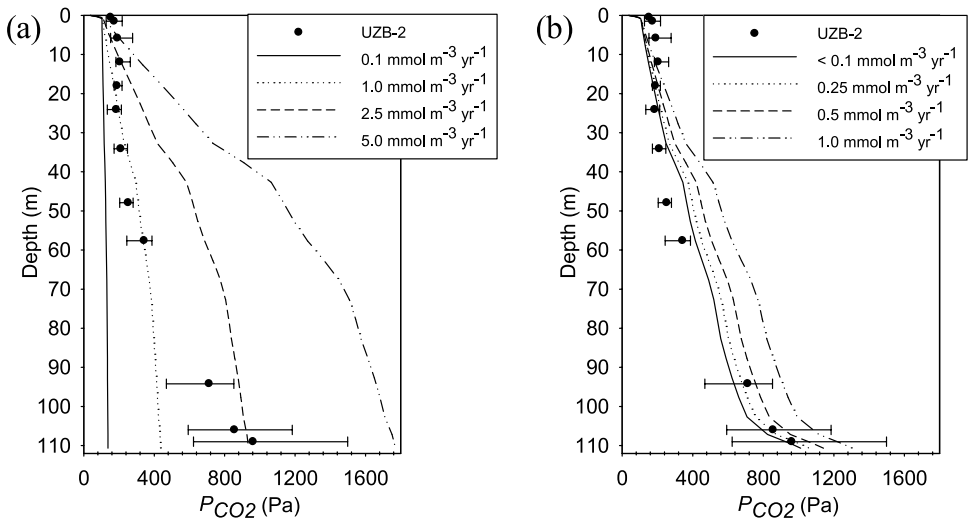

Figure 12. Modeled steady state P_{CO_2} profiles for (a) uniformly distributed CO_2 production (of variable magnitude) between 5 and 110 m, and (b) uniformly distributed CO_2 production (of variable magnitude) between 5 and 109 m plus a constant source of 0.1 mol CO_2 m^{-2} yr^{-1} above the water table.

profile. Comparison of the results from deep production at 0.1 mol m^{-3} yr^{-1} (base case) suggests that the basal respiration rate through the unsaturated zone at the ADRS is at least ~3 orders of magnitude lower than the CO_2 production near the water table and does not exceed 0.1 mmol m^{-3} yr^{-1} (Figure 12b).

4.5. Transient Model Results

[33] As mentioned previously, soil respiration rates vary seasonally, resulting in temporal changes in P_{CO_2} and $\delta^{13}C$ in the upper portion of the unsaturated zone. In contrast, $\delta^{14}C$ in CO_2 remains relatively constant year round. Transient simulations indicate how quickly P_{CO_2} and $\delta^{13}C$ profiles respond to changes in soil respiration. These simulations also illustrate propagation depths of seasonal P_{CO_2} and $\delta^{13}C$ fluctuations.

[34] The initial condition for all transient simulations is the steady state for the base case, which includes a soil respiration rate of 3 mol m^{-2} yr^{-1}, uniformly distributed in the upper 1 m. As an extreme case, respiration rate is increased to 7 mol m^{-2} yr^{-1} for an entire year (although such a sustained rate at the study site is unlikely given current conditions). To investigate the opposite extreme, respiration is eliminated for 1 year. Figure 13 shows the changes in P_{CO_2} and $\delta^{13}C$ from the steady state base case due to increased respiration for 1, 6, and 12 months (Figures 13a and 13b) as well as zero respiration (Figures 13c and 13d). Partial pressures of CO_2 near the surface more than double when subjected to increased soil respiration lasting 1 year. Conversely, pressures decrease to atmospheric levels after soil respiration ceases. Associated isotopic values near the surface drop to −19.5 ‰ $\delta^{13}C$ during of year of increased respiration and rise to −9.2 ‰ $\delta^{13}C$ (approaching atmospheric) during a year of zero respiration. Changes in P_{CO_2} diminish with depth and are nearly entirely damped below 30–35 m. Propagation depths for $\delta^{13}C$ fluctuations are smaller. Perturbations in the $\delta^{13}C$ profiles are minimal below depths of 8 m for the increased respiration and

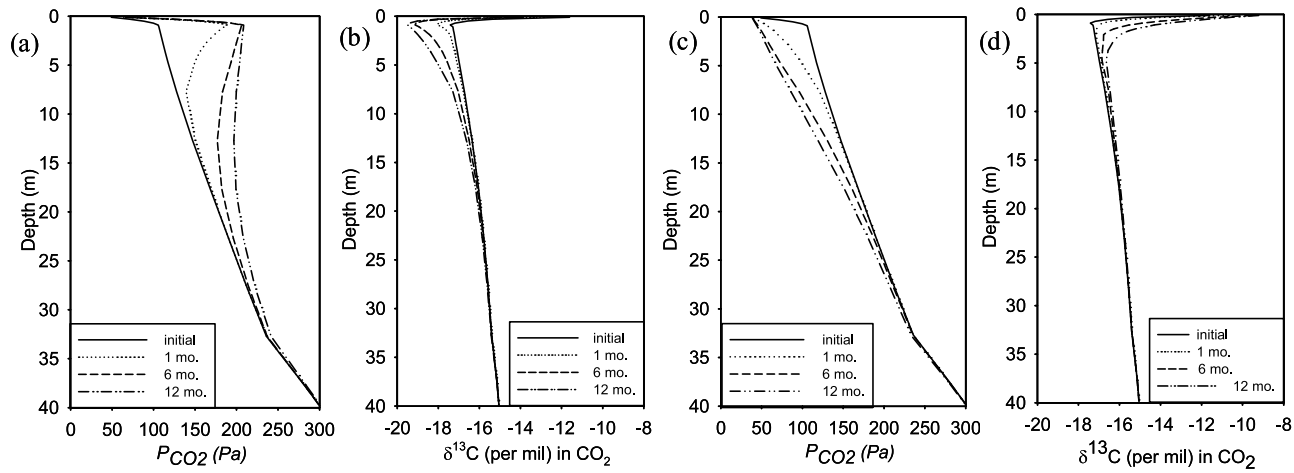

Figure 13. Modeled transient results for an increase in soil respiration from 3 to 7 mol CO_2 m^{-2} yr^{-1} on (a) P_{CO_2}, (b) $\delta^{13}C$ profiles, and a decrease in soil respiration from 3 to 0 mol CO_2 m^{-2} yr^{-1} on (c) P_{CO_2}, (d) $\delta^{13}C$ profiles. Only the upper 40 m is shown.

15 m for the zero respiration. The transient simulations show that the propagation depths of the simulated perturbations in the P_{CO_2} profile are more than twice those of the $\delta^{13}C$ profiles. The reservoir of dissolved inorganic carbon moderates the variation of $\delta^{13}C$ subjected to changes in soil respiration [*Parkhurst et al.*, 2000]. Dissolved carbon adjusts to maintain isotopic equilibrium with gas-phase CO_2.

5. Discussion

[35] Soil gas profiles from the ADRS indicate a source of $\sim$0.1 mol CO_2 m^{-2} yr^{-1} at the 110-m-deep water table. Simulations indicate that this deep source represents $\sim$3% of the total annual CO_2 production in the unsaturated zone with the balance derived from respiration in the upper 1 m. This ratio of deep-to-total CO_2 production in the unsaturated zone is comparable to the ratio of $\sim$2% (0.047 mol m^{-2} yr^{-1}) estimated at a semiarid site in Saskatchewan, Canada [*Keller and Bacon*, 1998]. Keller and Bacon attributed the deep production to georespiration (microbial consumption of ancient carbon) in the capillary fringe. Although similar in magnitude, deep CO_2 production at the ADRS differs (at least in part) with respect to origin. Observed calcite precipitation at the water table produces CO_2 from groundwater, providing an inorganic source of deep CO_2 at the ADRS. However, this inorganic source alone cannot account for the total 0.1 mol m^{-2} yr^{-1} flux estimated from model results. Calcite precipitation in a 1-m zone above the water table could not produce more than $\sim$0.1 mmol CO_2 m^{-2} yr^{-1}, given an evaporation rate of 0.1 mm yr^{-1}, which exceeds ADRS estimates of upward flux at the water table by an order of magnitude [*Walvoord et al.*, 2004]. Also, CO_2 derived from calcite precipitation in the (assumed) infinite aquifer would be limited by diffusion through water, which is $\sim$4 orders of magnitude lower than diffusion through air. The CO_2 concentration gradient in the aquifer required to support a 0.1 mol CO_2 m^{-2} yr^{-1} would be >250 mg $CO_{2(aq)}$ $L^{-1}m^{-1}$, which is unreasonably large.

[36] It is possible that georespiration serves as a major contributor to deep CO_2 production at the ADRS, based on the microbial counts that increase by over 3 orders of magnitude from the unsaturated zone to the saturated zone. Results of *Plough et al.* [2002] for an estuarine environment provide an upper limit on calculated respiration rates from microbial counts at 6.7×10^{-13} mol C CFU^{-1} yr^{-1}. This relation yields a maximum georespiration rate at the ADRS (given 10^6 CFU g^{-1} and a bulk density of 1.5×10^6 g m^{-3}) of $\sim$1 mol C m^{-3} yr^{-1}, which exceeds the calculated deep CO_2 production by an order of magnitude. A difficulty in attributing deep CO_2 production at the ADRS to georespiration involves the apparent lack of a long-term source of labile carbon. Unlike the site investigated by *Keller and Bacon* [1998], the subsurface environment at the ADRS contains low amounts of available organic carbon. We speculate that a slowly declining water table since the early Holocene may provide a mechanism to supply a continuous source of carbon for microbes in the capillary fringe.

6. Conclusions

[37] The following conclusions were found at the Amargosa Desert Research Site based on results presented in this paper. In addition to soil respiration, a combination of calcite precipitation and georespiration comprises a natural source of CO_2 in the unsaturated zone, amounting to $\sim$3% of the annual CO_2 production. This relatively small (0.1 mol m^{-2} yr^{-1}) deep CO_2 flux strongly controls P_{CO_2} and C-isotope distributions in the deep unsaturated zone. This sensitivity reflected in P_{CO_2} and C-isotope distributions imparts confidence in our estimates of deep CO_2 production. Explanation of the natural ^{14}C distribution in the unsaturated zone at the ADRS further requires application of the CO_2 sorption described by the generalized isotherm measured by *Striegl and Armstrong* [1990]. The historic variation in atmospheric ^{14}C enables estimation of soil carbon turnover times, which were constrained to be relatively rapid at the ADRS (<10 years). The conclusions drawn from this study have broader implications for deep CO_2 sources and the interpretation of C-isotope profiles in similar deep unsaturated zone settings. If a slowly declining water table is responsible for providing a continuous, but small, source of C in the capillary fringe to sustain a microbial respiration rate of $\sim$0.1 mol CO_2 m^{-2} yr^{-1} at the ADRS, major drops in water table level induced by groundwater pumping in arid southwestern basins or pervasive climate change could support a substantially larger georespiration rate, perhaps on a regional scale. Another broad implication derived from the ADRS study is that precipitation of calcite at the water table in arid settings (even when depth to water is more than 100 m) may be another mechanism for the formation of calcareous cementation of alluvial deposits. Pervasive cementation at depth could form hydraulic barriers to water movement.

[38] An understanding of CO_2 and C-isotope dynamics in unperturbed unsaturated-zone settings is needed to identify, interpret, and treat contaminated systems. Organic and inorganic processes affecting transport of gaseous radionuclides and volatile organic compounds are superimposed on natural processes. Understanding unsaturated-zone CO_2 dynamics under natural conditions is also necessary for assessing potential geologic sequestration of CO_2 [*Holloway*, 2001; *Lackner*, 2003; *Oldenburg and Unger*, 2003] as well as discriminating between natural and anthropogenic sources following sequestration. The analysis of P_{CO_2} and C-isotope distributions described herein provides a framework for evaluating fluxes of carbon in deep unsaturated zones.

[39] **Acknowledgments.** Donald Thorstenson and David Parkhurst developed the model used in the study and provided technical advice. Robert Oscarson and Marjorie Schulz helped obtain SEM images. William Evans, Herbert Haas, Robert Michel, and Joseph Whelan supplied data on carbon isotopes. Ronald Baker, Daniel Doctor, Edwin Weeks, and an anonymous reviewer provided helpful comments and suggestions on the manuscript. Support for the senior author was provided by the National Research Council through a postdoctoral appointment with the USGS. Additional support was provided by the USGS Ground-Water Resources Program, National Research Program, and the Toxic Substances Hydrology Program.

References

Andraski, B. J. (1997), Soil-water movement under natural-site and waste-site conditions: A multiple-year field study in the Mojave Desert, Nevada, *Water Resour. Res.*, *33*, 1901–1916.

Andraski, B. J., and D. A. Stonestrom (1999), Overview of research on water, gas, and radionuclide transport at the Amargosa Desert Research Site, Nevada, in *U.S. Geological Survey Toxic Substances Hydrology Program: Proceedings of the Technical Meeting, Charleston, South Carolina, March 8–12, 1999*, edited by D. W. Morganwalp and H. T. Buxton, *U.S. Geol. Surv. Water Resour. Invest. Rep.*, *99-4018C*, 459–465.

Bacon, D. H., and C. K. Keller (1998), Carbon dioxide respiration in the deep vadose zone: Implications for groundwater age dating, *Water Resour. Res.*, *34*, 3069–3077.

Baker, R. J., B. J. Andraski, M. A. Walvoord, D. A. Stonestrom, D. E. Prudic, and W. Luo (2003), Volatile organic compounds (VOCs) and elevated concentrations of carbon dioxide (CO_2) in unsaturated-zone vapors near a chemical and low-level radioactivity waste-disposal facility, Amargosa Desert Research Site, Nye County, Nevada, *Eos Trans. AGU*, *84*(46), Fall Meet. Suppl., Abstract H32A-0509.

Cerling, T. E., D. K. Solomon, J. Quade, and J. R. Bowman (1991), On the isotopic composition in soil carbon dioxide, *Geochim. Cosmochim. Acta*, *55*, 3403–3405.

Craig, H. (1957), Isotopic standards for carbon and oxygen and correction factors for mass-spectrometric analysis of carbon dioxide, *Geochim. Cosmochim. Acta*, *12*, 133–149.

Deines, P., D. Langmuir, and R. S. Harmon (1974), Stable carbon isotope ratios and the existence of a gas phase in the evolution of carbonate ground waters, *Geochim. Cosmochim. Acta*, *38*, 1147–1164.

Fischer, J. M. (1992), Sediment properties and water movement through shallow unsaturated alluvium at an arid site for disposal of low-level radioactive waste near Beatty, Nye County, Nevada, *U.S. Geol. Surv. Water Resour. Invest. Rep.*, *92-4032*, 48 pp.

Haas, H., D. W. Fischer, D. C. Thorstenson, and E. P. Weeks (1983), $^{13}CO_2$ and $^{14}CO_2$ measurements on soil atmosphere in the subsurface unsaturated zone in the Western Plains of the U.S., *Radiocarbon*, *23*, 301–314.

Hammermeister, D. P., D. O. Blout, and J. C. McDaniel (1985), Drilling and coring methods that minimize the disturbance of cuttings, core, and rock formation in the unsaturated zone, Yucca Mountain, Nevada, in *Proceedings of the Conference on Characterization and Monitoring of the Vadose (Unsaturated) Zone*, pp. 507–541, Natl. Water Well Assoc., Denver, Colo.

Harrill, J. R., J. S. Gates, and J. M. Thomas (1988), Major ground-water flow systems in the Great Basin region of Nevada, Utah, and adjacent states, *U.S. Geol. Surv. Hydrol. Invest. Atlas*, *HA-694-C*, 2 pp.

Hendry, M. J., J. R. Lawrence, B. N. Zanyk, and R. Kirkland (1993), Microbial production of CO_2 in unsaturated geologic media in a meso-scale model, *Water Resour. Res.*, *29*, 973–984.

Holloway, S. (2001), Storage of fossil fuel-derived carbon dioxide beneath the surface of the Earth, *Annu. Rev. Energy Environ.*, *26*, 145–166.

Johnson, M. J., C. J. Mayers, and B. J. Andraski (2002), Selected micrometeorological and soil-moisture data at Amargosa Desert Research Site in Nye County near Beatty, Nevada, 1998–2000, *U.S. Geol. Surv. Open File Rep.*, *02-348*, 21 pp. (Available at http://water.usgs.gov/pubs/of/2002/ofr02348/.)

Kaufmann, R. F., and S. J. Nacht (1989), Exploratory boring and monitoring well installation at the US Ecology RCRA Facility in Beatty, Nevada, *Rep. 88-02,107.18*, 83 pp., The Mark Group, Eng. and Geol., Inc., Las Vegas, Nev.

Keller, C. K. (1991), Hydrogeochemistry of a clayey till: 2. Sources of CO_2, *Water Resour. Res.*, *27*, 2555–2564.

Keller, C. K., and D. H. Bacon (1998), Soil respiration and georespiration distinguished by transport of vadose CO_2, $^{13}CO_2$, and $^{14}CO_2$, *Global Biogeochem. Cycles*, *12*, 361–372.

Kieft, T. L., J. K. Frederickson, J. P. McKinley, B. Bjornstad, S. A. Rawson, T. J. Phelps, F. J. Brockman, and S. M. Pfiffner (1995), Microbiological comparison within and across contiguous lacustrine, paleosol, and fluvial subsurface sediments, *Appl. Environ. Microbiol.*, *61*(2), 749–757.

Konopka, A., and R. Turco (1991), Biodegradation of organic compounds in vadose zone and aquifer sediments, *Appl. Environ. Microbiol.*, *57*(8), 2260–2268.

Lackner, K. S. (2003), A guide to CO_2 sequestration, *Science*, *300*, 1677–1678.

Laursen, S. (1991), On gaseous diffusion of CO_2 in the unsaturated zone, *J. Hydrol.*, *122*, 61–69.

Lawrence, J. R., B. N. Zanyk, M. J. Hendry, G. M. Wolfaardt, R. D. Robarts, and D. E. Caldwell (1993), Design and evaluation of a meso-scale model vadose zone and groundwater system, *Ground Water*, *31*, 455–466.

McConnaughey, T. A., J. F. Whelan, K. P. Wickland, and R. J. Moscati (1994), Isotopic studies of Yucca Mountain soil fluids and carbonate pedogenesis, in *High Level Radioactive Waste Management: Proceedings of the Fifth Annual International Conference, Las Vegas, Nevada*, pp. 2584–2589, Am. Nucl. Soc., Lagrange Park, Ill.

Millington, R. J. (1959), Gas diffusion in porous media, *Science*, *130*, 79–82.

Nichols, W. D. (1987), Geohydrology of the unsaturated zone at the burial site for low-level radioactive waste near Beatty, Nye County, Nevada, *U.S. Geol. Surv. Water Supply Pap.*, *2312*, 312 pp.

Oldenburg, C. M., and A. J. A. Unger (2003), On leakage and seepage from geologic carbon sequestration sites: Unsaturated zone attenuation, *Vadose Zone J.*, *2*, 287–296.

Parkhurst, D. L., and C. A. J. Appelo (1999), User's guide to PHREEQC (version 2)—A computer program for speciation, batch-reaction, one-dimensional transport, and inverse geochemical calculations, *U.S. Geol Surv. Water Resour. Invest. Rep.*, *99-4259*, 312 pp.

Parkhurst, D. L., D. C. Thorstenson, and K. L. Kipp (2000), Calculating carbon isotope compositions in an unsaturated zone with seasonally varying CO_2 production, in *Proceedings of the International Symposium on Hydrogeology and the Environment*, edited by Y. Wang and X. Liang, pp. 220–224, China Environ. Sci. Press, Beijing.

Plough, H., H. Zimmermann-Timm, and B. Schweitzer (2002), Microbial communities and respiration on aggregates in the Elbe Estuary, Germany, *Aquat. Microb. Ecol.*, *27*(3), 241–248.

Plummer, L. N., B. F. Jones, and A. H. Truesdell (1976), WATEQF: A FORTRAN IV version of WATEQ, a computer program for calculating chemical equilibria of natural waters, *U.S. Geol. Surv. Water Resour. Invest. Rep.*, *75-13*, 61 pp.

Plummer, L. N., E. C. Prestemon, and D. L. Parkhurst (1994), An interactive code (NETPATH) for modeling net geochemcial reactions along a flow path, version 2.0, *U.S. Geol. Surv. Water Resour. Invest. Rep.*, *94-4169*, 130 pp.

Plummer, M. A., L. C. Hull, and D. T. Fox (2004), Transport of carbon-14 in a large unsaturated soil column, *Vadose Zone J.*, *3*, 109–121.

Prudic, D. E. (1994), Estimates of percolation rates and ages of water in unsaturated sediments at two Mojave Desert sites, California-Nevada, *U.S. Geol. Surv. Water Resour. Invest. Rep.*, *94-4160*, 19 pp.

Prudic, D. E., and R. G. Striegl (1994), Water and carbon dioxide movement through unsaturated alluvium near an arid disposal site for low-level radioactive waste, Beatty, Nevada, *Eos Trans. AGU*, *75*(16), Spring Meet. Suppl., Abstract H31A-3.

Prudic, D. E., and R. G. Striegl (1995), Tritium and radioactive carbon (^{14}C) analyses of gas collected from unsaturated sediments next to a low-level radioactive-waste burial site south of Beatty, Nevada, April 1994 and July 1995, *U.S. Geol. Surv. Open File Rep.*, *95-741*, 7 pp.

Prudic, D. E., D. A. Stonestrom, and R. G. Striegl (1997), Tritium, deuterium, and oxygen-18 in water collected from unsaturated sediments near a low-level radioactive-waste burial site south of Beatty, Nevada, *U.S. Geol. Surv. Water Resour. Invest. Rep.*, *97-4062*, 32 pp.

Prudic, D. E., R. G. Striegl, R. W. Healy, R. L. Michel, and H. Haas (1999), Tritium and ^{14}C concentrations in unsaturated-zone gases at test hole UZB-2, Amargosa Desert Research Site, 1994–98, in *U.S. Geological Survey Toxic Substances Hydrology Program: Proceedings of the Technical Meeting, Charleston, South Carolina, March 8-12, 1999*, edited by D. W. Morganwalp and H. T. Buxton, *U.S. Geol. Surv. Water Resour. Invest. Rep.*, *99-4018C*, 475–484.

Reardon, E. J., G. B. Allison, and P. Fritz (1979), Seasonal chemical and isotopic variations of soil CO_2 at Trout Creek, Ontario, *J. Hydrol.*, *43*, 355–371.

Riggs, A. C., R. G. Striegl, and F. B. Maestas (1999), Soil respiration at the Amargosa Desert Research Site, in *U.S. Geological Survey Toxic Substances Hydrology Program: Proceedings of the Technical Meeting, Charleston, South Carolina, March 8-12, 1999*, edited by D. W. Morganwalp and H. T. Buxton, *U.S. Geol. Surv. Water Resour. Invest. Rep.*, *99-4018C*, 491–502.

Schimel, D., B. Braswell, E. Holland, R. McKeown, D. Ojima, T. Painter, W. Parton, and A. Townsend (1994), Climatic, edaphic, and biotic controls over storage and turnover of carbon in soils, *Global Biogeochem. Cycles*, *8*, 279–294.

Stonestrom, D. A., D. E. Prudic, and R. G. Striegl (1999), Isotopic composition of water in a deep unsaturated zone beside a radioactive-waste disposal area near Beatty, Nevada, in *U.S. Geological Survey Toxic Substances Hydrology Program: Proceedings of the Technical Meeting, Charleston, South Carolina, March 8-12, 1999*, edited by D. W. Morganwalp and H. T. Buxton, *U.S. Geol. Surv. Water Resour. Invest. Rep.*, *99-4018C*, 447–473.

Stonestrom, D. A., R. L. Michel, W. C. Evans, T. R. Smith, D. E. Prudic, R. G. Striegl, H. Hass, F. J. Brockman, and B. J. Andraski (2001), Carbon isotopes in unsaturated-zone gases and groundwater near a radioactive-waste disposal area, Amargosa Desert Research Site, Nye County, Nevada, *Eos Trans. AGU*, *82*(47), Fall Meet. Suppl., Abstract H52D-11.

Stonestrom, D. A., D. E. Prudic, R. J. Laczniak, and K. C. Akstin (2004), Tectonic, climatic, and land-use controls on groundwater recharge in an

arid alluvial basin: Amargosa Desert, U.S.A., in *Groundwater Recharge in a Desert Environment: The Southwestern United States*, *Water Sci. Appl. Ser.*, vol. 9, edited by J. F. Hogan et al., pp. 29–47, AGU, Washington, D. C.

Striegl, R. G., and D. E. Armstrong (1990), Carbon dioxide retention and carbon exchange on unsaturated Quaternary sediments, *Geochem. Cosmochim. Acta*, *54*, 2277–2283.

Striegl, R. G., and R. W. Healy (1990), Transport of $^{14}CO_2$ in unsaturated glacial and eolian sediments, in *Chemical Modeling of Aqueous Systems II*, *Am. Chem. Symp. Ser.*, vol. 416, edited by D. C. Melchior and R. L. Bassett, pp. 202–210, Am. Chem. Soc., Washington, D. C.

Striegl, R. G., D. E. Prudic, J. S. Duval, R. W. Healy, E. R. Landa, D. W. Pollock, D. C. Thorstenson, and E. P. Weeks (1996), Factors affecting tritium and 14-carbon distributions in the unsaturated zone near the low-level radioactive-waste burial site south of Beatty, Nevada, April 1994 and July 1995, *U.S. Geol. Surv. Open File Rep.*, *96-110*, 16 pp.

Stuiver, M., and H. Polach (1977), Reporting of ^{14}C data, *Radiocarbon*, *19*, 355–363.

Thorstenson, D. C., and D. L. Parkhurst (2004), Calculation of individual isotope equilibrium constants for geochemical reactions, *Geochim. Cosmochim. Acta*, *68*, 2449–2465.

Thorstenson, D. C., E. P. Weeks, H. Haas, and D. W. Fisher (1983), Distribution of gaseous $^{12}CO_2$, $^{13}CO_2$, and $^{14}CO_2$ in the sub-soil unsaturated zone of the western U.S. Great Plains, *Radiocarbon*, *25*, 315–346.

Thorstenson, D. C., E. P. Weeks, H. Haas, E. Busenberg, L. N. Plummer, and C. A. Peters (1998), Chemistry of unsaturated zone gases sampled in open boreholes at the crest of Yucca Mountain, Nevada: Data and basic concepts of chemical and physical processes in the mountain, *Water Resour. Res.*, *34*, 1507–1529.

Trumbore, S. E. (2000), Age of soil organic matter and soil respiration: Radiocarbon constraints on belowground C dynamics, *Ecol. Appl.*, *10*, 399–411.

Trumbore, S. E., E. A. Davidson, P. B. de Camargo, D. C. Nepstad, and L. A. Martinelli (1995), Belowground cycling of carbon in forests and pastures of eastern Amazonia, *Global Biogeochem. Cycles*, *9*, 515–528.

Urey, H. C. (1947), The thermodynamic properties of isotopic substances, *J. Chem.*, 562–581.

Walvoord, M. A., D. A. Stonestrom, B. J. Andraski, and R. G. Striegl (2004), Constraining the inferred paleohydrologic evolution of a deep unsaturated zone in the Amargosa Desert, *Vadose Zone J.*, *3*, 502–512.

Wang, Y., R. Amundson, and S. Trumbore (1996), Radiocarbon dating of soil organic matter, *Quat. Res.*, *49*, 282–288.

Wood, B. D., C. K. Keller, and D. L. Johnstone (1993), In situ measurement of microbial activity and controls on microbial CO_2 production in the unsaturated zone, *Water Resour. Res.*, *29*, 647–659.

Wood, W. W. (1976), Guidelines for collection and field analysis of groundwater samples for selected unstable constituents, *U.S. Geol. Surv. Tech. Water Resour. Invest. Book 1, Chap. D2*.

Wood, W. W., and M. J. Petraitis (1984), Origin and distribution of carbon dioxide in the unsaturated zone of the southern high plains of Texas, *Water Resour. Res.*, *20*, 1193–1208.

D. E. Prudic, U.S. Geological Survey, Carson City, NV 89706, USA.

D. A. Stonestrom, U.S. Geological Survey, Menlo Park, CA 94025, USA.

R. G. Striegl and M. A. Walvoord, U.S. Geological Survey, Lakewood, CO 80225, USA. (walvoord@usgs.gov)